A Short-Time Diffusion Correlation for Hydrogen-Induced Crack Growth Kinetics

W. W. GERBERICH, Y. T. CHEN, AND C. ST. JOHN

Analysis of hydrogen-stress field interactions have led to kinetic criteria for slow crack growth. Using both elastic and plastic stress fields under opening-mode loading, criteria for stage I, II, III growth are developed in terms of the pressure tensor gradient at the crack tip. It is proposed that stage I (stress-intensity dependent) growth kinetics are predominantly controlled by the elastic stress field while stage II (nearly stress-intensity independent) kinetics are controlled by the plastic stress field. Measurements of slow crack growth in cathodically-charged AISI 4340 steel verify the overall aspects of the correlation. Detailed measurement and analysis of the increase in crack-tip radius with increasing applied stress intensity have led to a proposed decrease in crack growth rate during stage II growth. Some experimental evidence corroborates this later hypothesis and is consistent with long range diffusional flow of hydrogen as the controlling mechanism for crack growth kinetics.

THERE is nearly unanimity[1-8] that the hydrostatic stress field at the tip of a crack is a major component if not the controlling parameter in hydrogen embrittlement processes. For example, stress field effects on the threshold stress intensity for cracking,[3,4] on cracking at zero isoclinics,[5] on hydrogen induced cracking at grain-boundary precipitates[6] and on the general interaction energy for interstitials[7,8] have been discussed at some length. However, there have been no quantitative attempts to correlate the crack velocity to short-time diffusion effects associated with stress-induced migration of hydrogen. Although Liu[7] addressed the kinetic problem, it was in a very general way and the form of the reaction rate equation was assumed.

The present paper is an outgrowth of a theoretical approach for correlating crack growth kinetics using both elastic and elastic-plastic stress fields.[9] In the previous paper, the three stages of crack growth rate, as illustrated in Fig. 1, were briefly discussed. Of particular interest was that the stage II stress-intensity independent growth process was exhibited by a host of materials under a large number of environmental test conditions. This might indicate that it is a general crack-tip stress field effect rather than a material-environment effect. The present study had three purposes:

(i) To investigate in more detail stage I, stage II and stage III crack growth kinetics, with emphasis on stage II.

(ii) To investigate the effect of tempering and hence yield strength on crack growth kinetics.

(iii) To ascertain the reasonableness of a fracture mechanics correlation which describes kinetics solely in terms of the rate of hydrogen diffusion to the crack tip.

W. W. GERBERICH and Y. T. CHEN are Associate Professor and Graduate Student, respectively, in the Department of Chemical Engineering and Materials Science at the University of Minnesota, Minneapolis, MN 55455. C. ST. JOHN, Research Scientist, Centre des Materiaux de l'Ecole des Mines, Corbeil-Essone, France. Y. T. CHEN'S participation is in partial fulfillment of the M.S. Degree at the University of Minnesota.

Manuscript submitted October 30, 1974

It should be emphasized that this is not a physical model since there is no failure criterion in terms of why a certain hydrogen level might be required to nucleate fracture over a specified microstructural region. In this sense, it is an extension of the fracture mechanics concept for threshold stress intensity.[4]

MATERIALS AND PROCEDURES

The materials and procedures were largely identical to those used in a previous investigation.[4] For the material, high strength 4340 steel had been austenitized at 850°C (1123 K) for one hour, oil-quenched and tempered in the range of 200 to 500°C (473 to 773 K). Characterization of the resulting strength properties, as completed since the last investigation are shown in

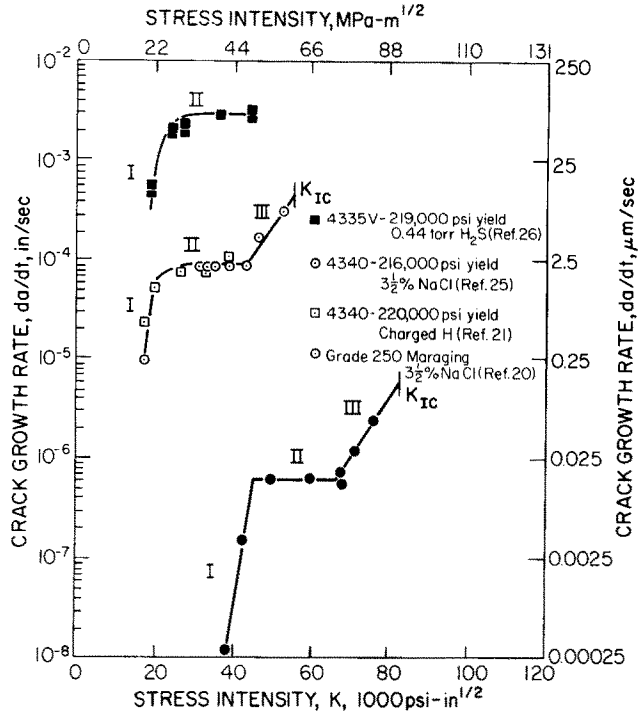

Fig. 1—Material, environment and stress intensity level effects on crack growth rate (Courtesy of ASM, Ref. 9).

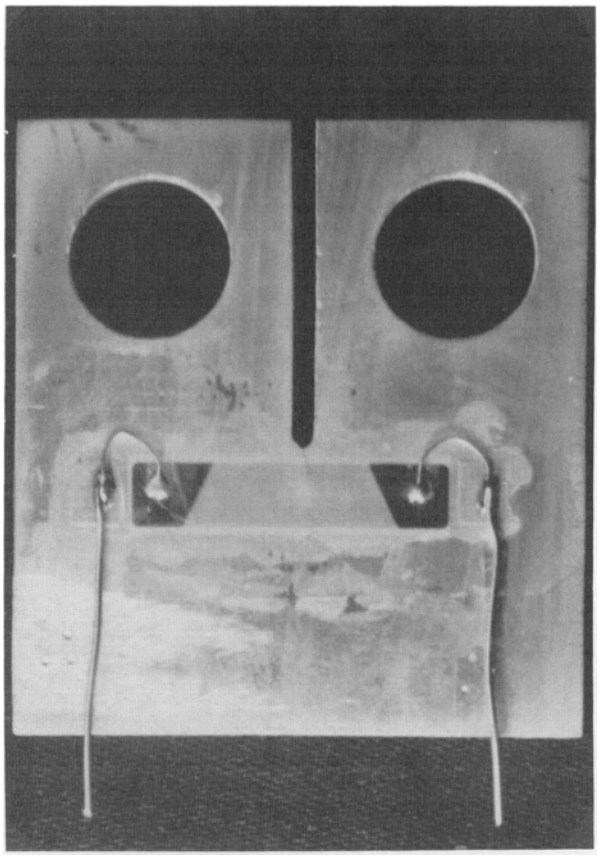

(a)

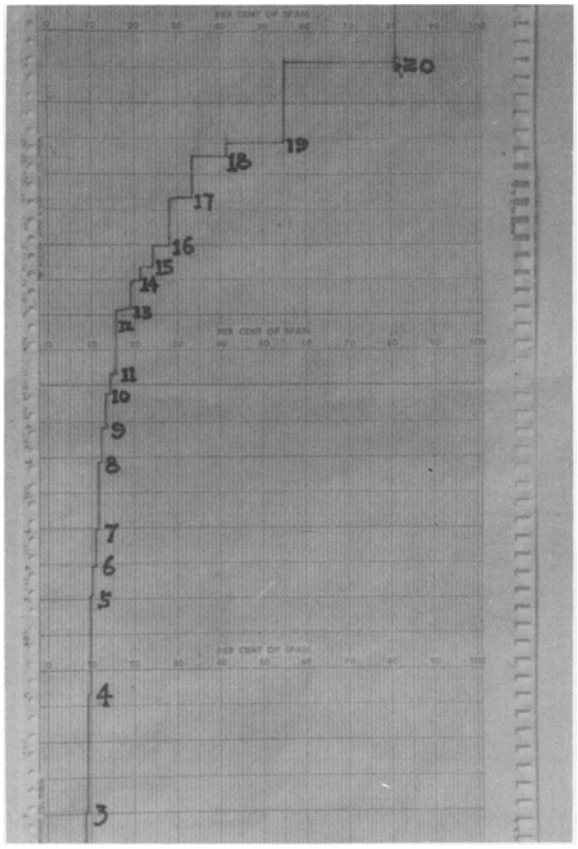

(b)

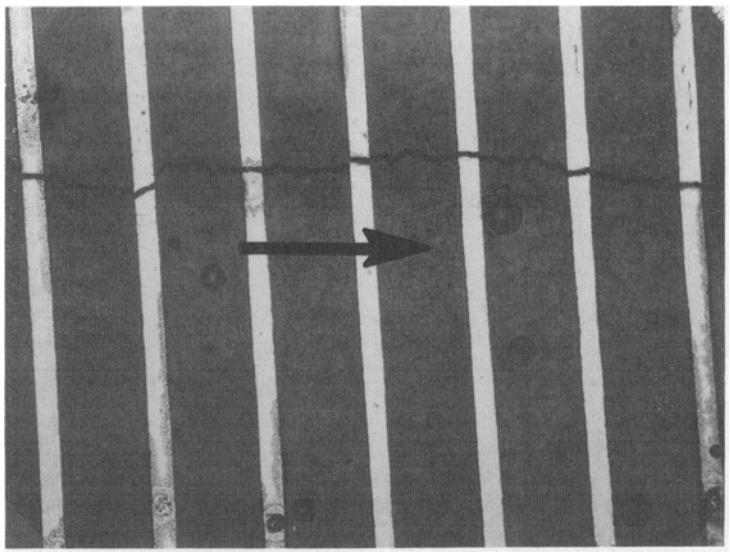

(c)

Fig. 2–Details of the crack growth measurement technique: (*a*) compact tension fracture specimen; (*b*) strip chart of time versus resistance from crack propagation gages; (*c*) details of crack propagation gage.

Table I. Compact tension specimens were first prepared by fatigue pre-cracking at a ΔK of 10,000 psi-in$^{1/2}$ (11 MPa-m$^{1/2}$). They were then hydrogen charged and cadmium plated until $C_0 \simeq 2.6$ ppm H, based upon hydrogen entry into 200,000 psi (1380 MPa) yield strength 4340 steel. After baking at 150°C to uniformly distribute the hydrogen, the 19 mm thick specimens were fitted with crack propagation gages having 20 grid lines at 250 μm intervals. The gage can be considered as a number of resistor strands connected in parallel. When bonded to a crack-line loaded specimen, progression of a crack through the gage will cause successive open-circuiting of the strands, producing an increase in total resistance. Such an example of a gage and the resulting stepped-resistance curve is shown in Fig. 2. Since Fig. 2(*b*) is a time-based strip chart, the average crack growth rate over each 250 μm interval may be determined.

Crack growth rate studies were attempted for 200 (473), 300 (573), 400 (673), 480 (753), and 550°C (473 K) temper due to cracking during charging. The majority of the data reported will be for the plane strain condi-

Table I. Composition and Tensile Properties of AISI 4340

Composition, wt. pct							
C	P	S	Mn	Si	Cr	Mo	Ni
0.40	0.035	0.04	0.80	0.21	0.80	0.25	1.9

Tensile Properties*

Material and Temper	Yield Strength 1000 psi	Yield Strength (MPa)	Ultimate Strength 1000 psi	Ultimate Strength (MPa)	Elongation pct
4340/200°C	223	(1540)	280	(1930)	5.0
4340/300°C	208	(1440)	241	(1660)	5.0
4340/400°C	198	(1370)	217	(1500)	5.0
4340/480°C	173	(1195)	187	(1290)	7.0
4340/550°C	159	(1100)	171	(1180)	7.5

*Average of Duplicate Tests.

tion (19 mm thick) tempered at 300 to 550°C (573 to 823 K). Applied stress intensities, were calculated from the recorded load, P, and the crack length, a, using

$$K_I = \frac{P(a)^{1/2}}{BW} Y \qquad [1]$$

where $Y = 29.6 - 185.5(a/w) + 665.7(a/w)^2 - 1017(a/w)^3 + 639(a/w)^4$ and BW refer to the specimen thickness and width.

As the investigation proceeded, it became apparent that the bluntness of the crack-tip radius might be of importance with respect to the stress field at the crack tip. Therefore, a replica technique was employed to give measurements of crack-tip radius as a function of yield strength and stress intensity. Specimens tempered at 200 (473), 480 (753) and 550°C (823 K) were polished to a 6 μm finish. They were then held at constant stress intensities ranging from 20,000 to 100,000 psi-in$^{1/2}$ (21.8 to 109 Mpa-m$^{1/2}$) and cellulose acetate film was applied to the crack tip region. The tape was then removed from the polished surface, placed on a glass plate and bombarded with carbon and gold in an evaporator. In this way, both scanning and light microscopy could be utilized to observe the crack-tip profiles.

RESULTS

Crack growth rate as a function of applied stress intensity level is shown for four temper conditions in Fig. 3. The points plotted on the abscissa represent threshold stress intensities. It is seen that the three stages of crack growth are in evidence to varying degrees depending upon the tempering temperature. There is little evidence of stage III for the lower tempers, since their low fracture toughness caused instability at the end of stage II. At the other extreme, there is no evidence of stage I crack growth for the conditions with the higher tempering temperatures. This indicates that threshold immediately proceeded to stage II growth. There was a tendency for crack growth rate to increase with increasing stress intensith level for stage I and III growth but not for stage II.

Considering stage II growth in more detail, it is first significant that $(da/dt)_{II}$ decreased by more than two orders of magnitude as the tempering temperature increased. As this represented only a 50,000 psi (340 MPa) drop in yield strength, a mechanism only dependent upon yield strength level would require a $(\sigma_{ys})^{17}$ dependence to account for the change in kinetics. As this seems unlikely and in fact contradictory to what is found in maraging steels,[10] a different effect of tempering or aging on the growth kinetics must be invoked. The other point is that $(da/dt)_{II}$ tends to decrease slightly with increasing stress intensity. For the 480°C (753 K) tempered condition, the details are shown in expanded form in Fig. 4. Also shown here are additional data of a 300°C (573 K) tempered sample, 9 mm thick. First, note that there are intermittent slow and fast regions of growth with solid straight lines noting the chronological order of events. It is possible that some of the intermittent nature is due to the fact that the growth measurement is at the surface and not over the entire cross section. However, detailed crack-opening-displacement measurements of similar high strength steels[11] have noted similar alternate slow and burst regions of growth. The important point to the present discussion is that there is a tendency for both the peaks and the valleys to decrease with increasing K_I. To make the point more vivid, all data for a number of specimen thicknesses were summarized as follows. The data from one peak through a valley to the next peak were averaged with respect to $\overline{K_I}$ and $(\overline{da/dt})_{II}$. These are plotted for the 300°C (573 K) temper condition in Fig. 5. Again, it is seen that $(da/dt)_{II}$ decreases with increasing K_I. The effect shows up more at the smaller thickness due to a transition from plane strain to plane stress and the corresponding change in the triaxial stress field associated with that.[9]

One can see the ramifications of varying stress in-

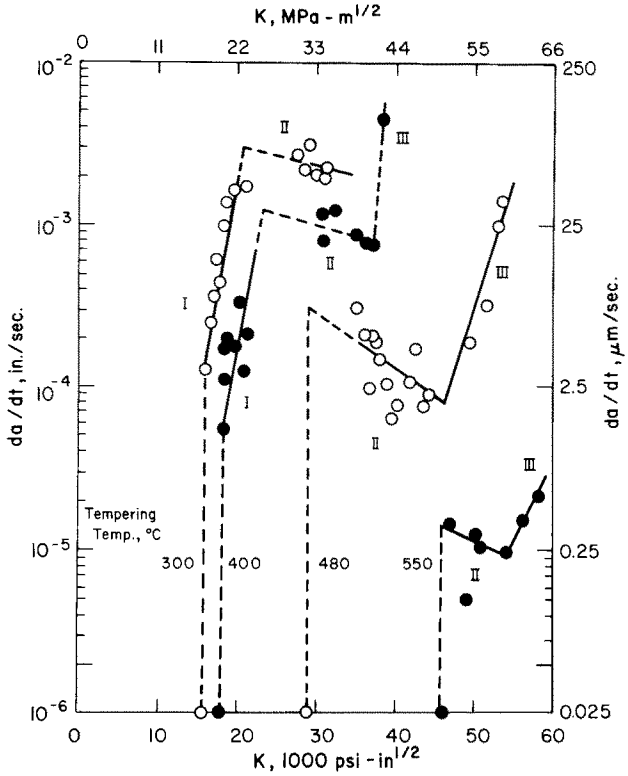

Fig. 3—Crack growth rate as a function of applied stress intensity for four different temper conditions of 4340 steel.

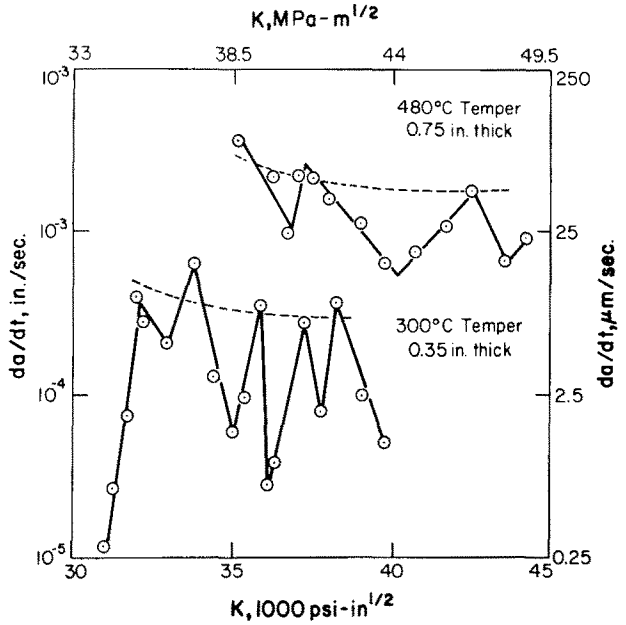

Fig. 4—Details of the stage II crack growth rate process.

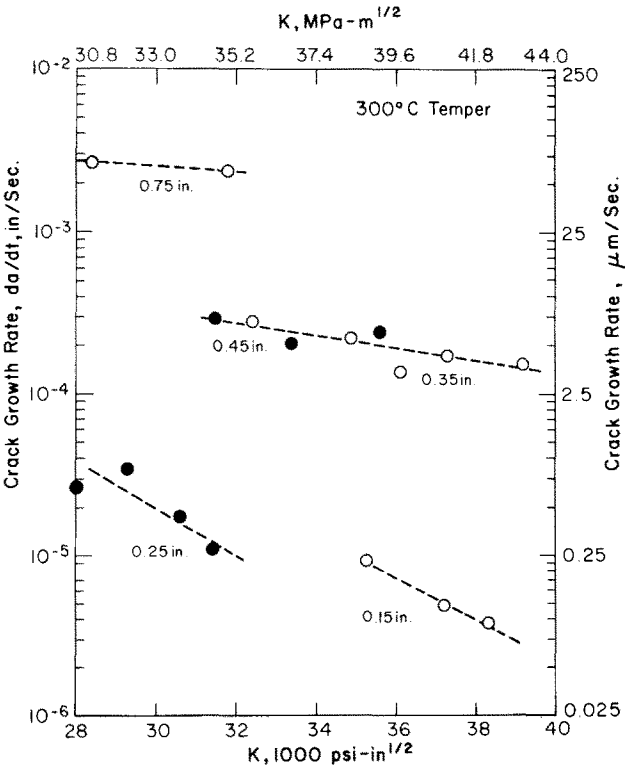

Fig. 5—Average crack growth rate in stage II as a function of stress intensity for several thicknesses of the 300°C (573K) tempered condition.

tensity level on the fracture surface morphology in Fig. 6. Near the threshold and for stage I growth, the crack extension process was nearly 100 pct intergranular. It should be noted that the intergranular facet size was on the order of 10 μm in all cases. During stage II growth, as the stress intensity increased, there was a tendency to have more ductile rupture in combination with the intergranular process. Finally, in stage III as instability was approached, the ductile rupture process became predominant as indicated in Fig. 6(*c*) and (*d*).

DISCUSSION

The theoretical approach here is one discussed previously[9] but given here in somewhat greater depth. First, the pressure tensor gradient, dp/dx, acts as a driving force for hydrogen diffusion so that the diffusive flux may be either into or out of the crack tip, depending upon the sign of the gradient. To illustrate this, normal stresses calculated from elasticity and plasticity theory[12,13] are shown in Fig. 7 for $K_I/\sigma_{ys} = 0.15$. Note that these are stresses along the line of the crack at $\theta = 0$ deg. First, one sees that $\sigma_{ii}/3$ increases as $1/\sqrt{x}$ as the crack tip is approached in the elastic region. If the material had been completely elastic, then dp/dx would have been increasingly negative toward the crack tip. This would drive hydrogen to the left (in Fig. 7) towards the crack tip. On the other hand, in the plastic region, dp/dx is positive and hydrogen is driven to the right away from the crack tip. If one only considers the first order interaction effects and ignores concentration gradient effects, then the maximum hydrogen concentration as well as the maximum triaxial stress would occur at X_{cr}, the elastic-plastic boundary,* Calculations of dp/dx were carried out at a stress intensity level where slow crack growth readily occurred. For those conditions with yield strengths near 200,000 psi (1380 MPa), this was typically at $K \simeq 30{,}000$ psi-in$^{1/2}$ (33 MPa-m$^{1/2}$). In the elastic-plastic case shown in Fig. 7, it is evident that hydrogen would collect at X_{cr}, which in this case is 7×10^{-4} in. or 17.8 μm. Over the range of stress intensities encountered (~15-60 MPa-m$^{1/2}$), the value of X_{cr} would vary from about 6 μm to 52 μm. As these extremes bracket the actual grain size (10 μm), and since the fracture process is predominantly intergranular, it is reasonable to use the grain diameter as a size parameter in estimating crack growth kinetics.

*More recent analyses have shown that X_{cr} would lie within the plastic zone. The ramifications of this on Fig. 7 and the subsequent theoretical developments is discussed under further considerations.

In Fig. 7 where $K_I = 30{,}000$ psi-in$^{1/2}$ (33 MPa-m$^{1/2}$), the magnitude of dp/dx is almost exactly the same at X_{cr} when comparing elastic and plastic calculations, *i.e.* 2.20×10^8 psi/in (0.595×10^8 MPa/m) *vs* -2.16×10^8 psi/in (0.585×10^8 MPa/m). One can also show that for stress intensities about half this, that $(dp/dx)_{\text{elastic}} \simeq 2\,(dp/dx)_{\text{plastic}}$ while for stress intensities double this, $(dp/dx)_{\text{elastic}} \simeq \frac{1}{2}(dp/dx)_{\text{plastic}}$. It becomes clear that if cracking nucleates in front of the main crack font, then the diffusive flux which controls kinetics may be elastically controlled at low stress intensities and plastically controlled at high stress intensities. We propose that stage I crack growth kinetics are elastically controlled and stage II kinetics are plastically controlled.

i) Elastic Considerations for Stage I

At relatively low stress intensities, either intergranular or quasi-cleavage fractures have been observed.[14] Stage I growth could be associated with primarily elastic loading where the plastic zone is very small. Here, the long range diffusivity of hydrogen would be controlled by the elastic stress distribution. This is schematically depicted in Fig. 8(*a*). For

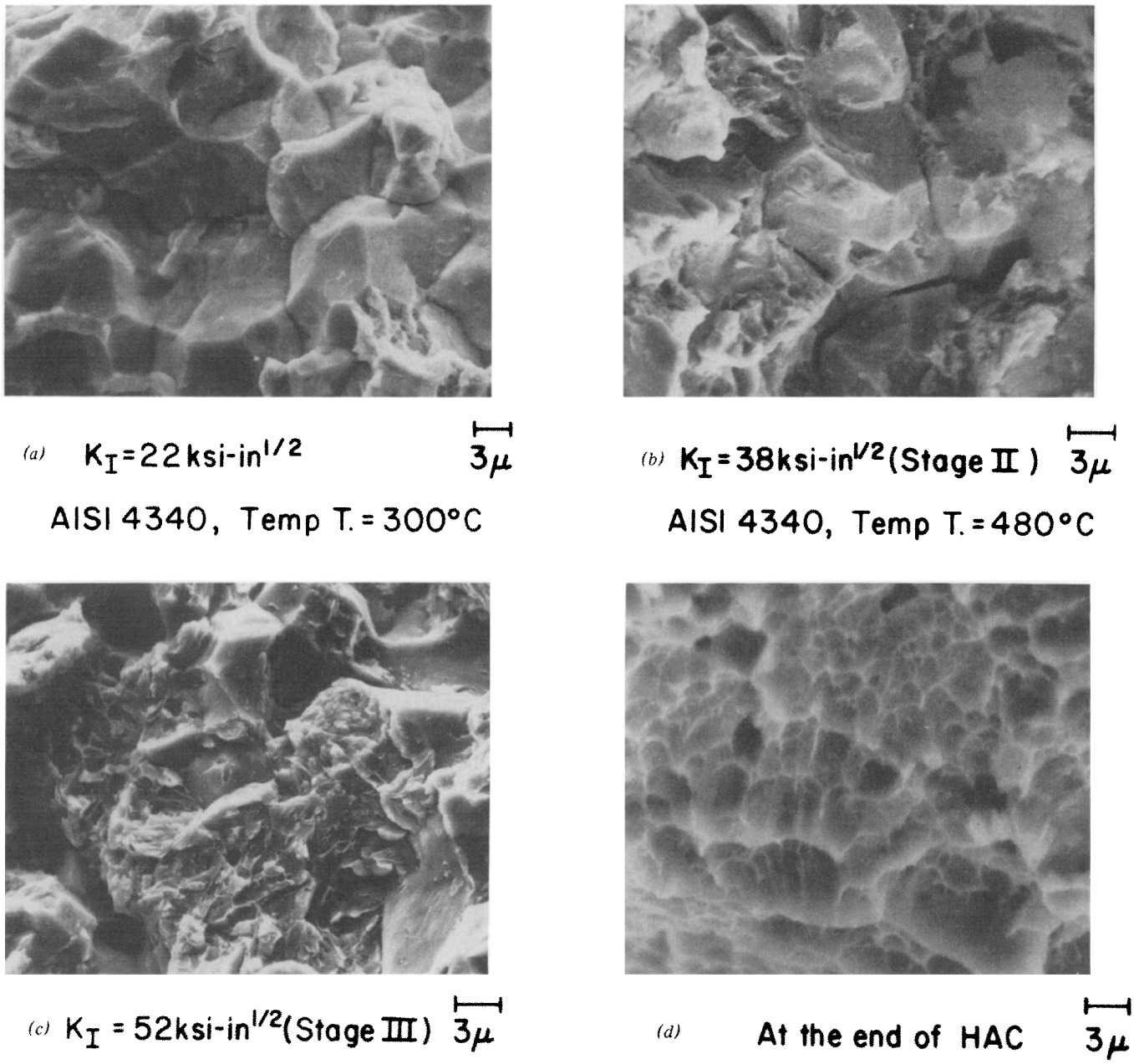

Fig. 6–Scanning electron microscopy showing intergranular fracture with increasing amounts of ductile rupture at higher stress intensities: (*a*) 300°C (573K); (*b*) (*c*) (*d*) 480°C (753K).

the model, the following assumptions are made:

i. The plastic zone is within a region less than a grain size.

ii. The crack nucleates over one grain, d.

iii. The hydrogen collects in this grain from the immediate surrounding grains.

iv. The crack grows intergranularly, one grain at a time.

v. The growth step occurs when $C_0 \rightarrow C_{cr}$.

vi. Short-time diffusion kinetics are applicable.

Next, consider a single hydrogen atom moving at velocity, v, taking a time, d/v, to move from one grain to the next. If v is the average velocity of the hydrogen atoms and d is the average distance moved, then the concentration increases in the grain at the crack tip by $3C_0vt/d$. That is, the shaded region in Fig. 8(*a*) adds to the original concentration of the grain contiguous to the crack tip depending on drift velocity and time. This concept is detailed in Appendix A. If the time between crack jumps is Δt_s, it follows that

$$C_{cr} \simeq C_0 + \frac{3C_0v\Delta t_s}{d} \qquad [2]$$

Since the drift belocity for short time diffusion is

$$v = \frac{D_A}{RT}\,\bar{V}_H\,\frac{dp}{dx} \qquad [3]$$

it follows from Eqs. [2] and [3] that the time between jumps is

$$\Delta t_s = \frac{(C_{cr} - C_0) dRT}{3C_0 D_A \overline{V}_H dp/dx} \quad [4]$$

On a local scale, da/dt is simply the average incremental crack jump divided by the average time between jumps. It follows that

$$\frac{da}{dt} = \frac{l_{cr}}{\Delta t_s} = \frac{3C_0 D_A \overline{V}_H dp/dx}{(C_{cr} - C_0) RT} \quad [5]$$

From the mean value theorem* one can calculate the

*See Appendix B.

average value of dp/dx over the contributing region indicated in Fig. 8(*a*) by using the opening mode solution. This finally leads to

$$\left.\frac{dp}{dx}\right|_{\text{Avg.}} = \frac{2K(1+\nu)}{9d^{3/2}} \quad [6]$$

From Eqs. [5] and [6], a first approximation for stage I growth is

$$\left(\frac{da}{dt}\right)_{\text{I}} = \frac{2(1+\nu) C_0 D_A \overline{V}_H K}{3d^{3/2} RT (C_{cr} - C_0)} \quad [7]$$

It is seen that this approach predicts a linear increase in da/dt with applied stress intensity for stage I growth.

ii) Plastic Considerations for Stage II

First, consider when the plastic zone exceeds several grains as indicated in Fig. 8(*b*). The crack tip blunts and a plastically contrained region forms with a stress distribution similar to that in Fig. 7. Now, hydrogen flows away from the crack tip to approximately a grain length in front. Other assumptions ii through vi are the same as above. Over the range of stress intensities normally encountered, ρ might range from a fraction of a grain to about a grain size in radius. This, in conjunction with Eq. [8], the mean value

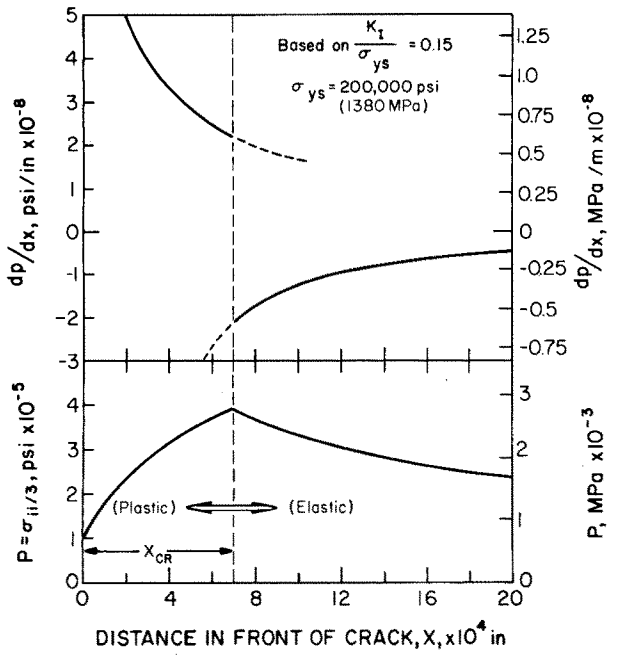

Fig. 7—Elastic and plastic pressure tensors and pressure tensor gradients for typical conditions appropriate to stage II growth.

theorem,* and the limits depicted in Fig. 8(*b*), leads to

*See Appendix B.

$$\left.\frac{dp}{dx}\right|_{\text{Avg.}} \simeq \frac{3\sigma_{ys}}{2d} \quad [8]$$

From Eqs. [5] and [8], a first approximation for stage II is

$$\left(\frac{da}{dt}\right)_{\text{II}} = \frac{9C_0 D_A \overline{V}_H \sigma_{ys}}{2dRT(C_{cr} - C_0)} \quad [9]$$

The main difference between this and stage I is that the triaxial stress gradient increases with stress intensity for I but is independent of stress intensity for II. This would then predict that crack growth kinetics are essentially independent of applied stress intensity during stage II growth, as has been observed.

iii) Plastic Considerations for Stage III

At higher stress intensities approaching K_{IC}, the plastic considerations for diffusion could remain the same. However, if the fracture mode changes to a ductile rupture process, then the distance the crack jumps in a single step would not be controlled by the grain size. Thus, in stage III, it is considered that the crack nucleates intergranularly, but the growth step is governed largely by ductile rupture considerations. In this case the growth process would be partially intergranular and partially ductile rupture as depicted in Fig. 8(*c*). The crack jump distance might be given by

$$l_{cr} \simeq \frac{K^2}{\sigma_{ys} E} \quad [10]$$

With the other assumptions remaining nearly the same, this leads to stage III growth kinetics. From Eqs. [5], [8] and [10],

$$\left(\frac{da}{dt}\right)_{\text{III}} \simeq \frac{9C_0 D_A \overline{V}_H K^2}{2Ed^2 RT(C_{cr} - C_0)} \quad [11]$$

It is seen for stage III that growth rate reverts to a highly dependent stress-intensity process.

iv) Transitional Behavior for da/dt

One might expect that if these correlations had any validity, that the transitions from stage I to stage II growth and stage II to stage III growth might be significant. The first is simply obtained by equating Eqs. [7] to [9] giving

$$K_{\text{I}\rightarrow\text{II}} = 5.2 d^{1/2} \sigma_{ys} \quad [12]$$

Note that this says the transition occurs when $d = (1/27)(K/\sigma_{ys})^2$. Since the plane strain plastic zone size is about $(1/6\pi)(K/\sigma_{ys})^2$, the picture shown in Fig. 8(*b*) is not inconsistent. For the second transition, equating Eqs. [9] and [11] gives

$$K_{\text{II}\rightarrow\text{III}} = [\sigma_{ys} E d]^{1/2} \quad [13]$$

Again, this is consistent with Fig. 8 since Eq. [13] would indicate that stage III growth would predominate when $K_{\text{I}}^2/\sigma_{ys} E > d$, *i.e.* $l_{cr} > d$.

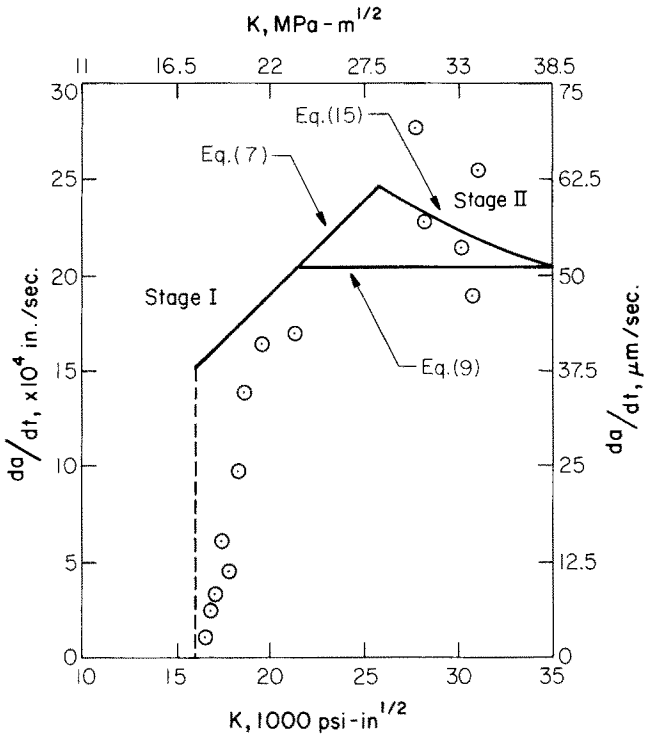

Fig. 9—Application of the theoretical correlation to stage I and II growth rates observed for the 300°C (573K) tempered condition.

tip which could produce a difference in both void content and dislocation density when loaded.[19] This, in turn, would affect trapping.

The actual effect of tempering on D_A at the crack tip is only speculation at this time and systematic studies of permeation on tempered and cold-worked, tempered structures are required for further elucidation.

In lieu of this, what can be assessed are those transitions which are nearly independent of the term $[C_0/(C_{cr} - C_0)]D_A$. One may note that in Eqs. [7], [9], [11], this term is contained in each. Furthermore, one might assume that in a given material, on either side of a transition, *e.g.* I → II, that $D_A[C_0/(C_{cr} - C_0)]_{\mathrm{I}} \simeq D_A[C_0/(C_{cr} - C_0)]_{\mathrm{II}}$. This would then allow Eqs. [7] and [9] to be assessed for the data of other investigations as well as this one. First, consider the transition from stage I to II. The data from Fig. 3 along with a previous tabulation[9] are shown in Table II. Although it is seen that $K_{\mathrm{I}\rightarrow\mathrm{II}}/\sigma_{ys}$ ranges from 0.007 to 0.03 $m^{1/2}$, the majority of the data are grouped near 0.016 $m^{1/2}$. Using the typical grain diameter 10 μm for this study, a calculation of $K_{\mathrm{I}\rightarrow\mathrm{II}}/\sigma_{ys}$ from Eq. [12] gives 0.016 $m^{1/2}$ (0.104 $in^{1/2}$) which is in excellent agreement.

A similar tabulation for the transition from stage II to stage III is shown in Table III. For $K_{\mathrm{II}\rightarrow\mathrm{III}}/(\sigma_{ys}E)^{1/2}$, the values range from 0.0023 to 0.0041 $m^{1/2}$ but on the average is 0.0033 $m^{1/2}$ (0.0205 $in^{1/2}$). According to Eq. [13], this ratio should correspond to $d^{1/2}$, which would be 0.0032 $m^{1/2}$ (0.02 $in^{1/2}$) if a typical grain size of 10 μm (4×10^{-4} in.) is utilized. These excellent correlations lend considerably credence to the continuum mechanics approach even if the over all understanding of the diffusivity and, more importantly, the actual fracture mechanism is lacking.

Table II. Transition from *K* Dependent (I) to *K* Independent (II) Growth Kinteics

Material	Yield Strength 1000 psi (MPa)	$K_{\mathrm{I}\rightarrow\mathrm{II}}$ 1000 psi-in$^{1/2}$ (MPa-m$^{1/2}$)	$K_{\mathrm{I}\rightarrow\mathrm{II}}/\sigma_{ys}$ (in$^{1/2}$)	(m$^{1/2}$)	Ref.
4340 (300°C)	208 (1440)	20.5 (22.6)	0.098	(0.016)	This
4340 (400°C)	198 (1370)	23 (25.3)	0.116	(0.018)	Study
4340 (480°C)	173 (1195)	No Stage I	–	–	
4340 (550°C)	159 (1100)	No Stage I	—	–	
4340	194 (1340)	24 (26.4)	0.124	(0.020)	23
4340	200 (1380)	~22 (24.2)	0.110	(0.017)	1
4340	216 (1490)	25 (27.5)	0.116	(0.018)	20
4340	219 (1510)	27 (29.7)	0.123	(0.020)	26
300M	233 (1610)	~22 (24.2)	0.095	(0.015)	20
9Ni-4Co-0.45C	236 (1630)	25 (27.5)	0.106	(0.017)	23
250 Maraging	246 (1700)	46 (50.6)	0.188	(0.030)	25
300 Maraging (460°C/3)	263 (1810)	13 (14.3)	0.050	(0.008)	23
300 Maraging	284 (1960)	22 (24.2)	0.078	(0.012)	23
300 Maraging (482°C/6)	286 (1970)	~35 (38.5)	0.122	(0.020)	25
300 Maraging (482°C/8)	316 (2180)	20 (22.0)	0.063	(0.010)	23
350 Maraging (475°C/8)	299 (2060)	>30 (33.0)	>0.101	(0.016)	23
350 Maraging	330 (2280)	15 (16.5)	0.046	(0.007)	23
Average =			0.102	(0.016)	

Table III. Transition from Stage II to Stage III Growth Kinetics

Material	Yield Strength 1000 psi (MPa)	$K_{\mathrm{II}\rightarrow\mathrm{III}}$ 1000 psi-in$^{1/2}$ (MPa-m$^{1/2}$)	$K_{\mathrm{II}\rightarrow\mathrm{III}}/(\sigma_{ys}E)^{1/2}$ (in$^{1/2}$)	(m$^{1/2}$)	Ref.
4340 (300°C)	208 (1440)	No Stage II	–	–	
4340 (400°C)	198 (1370)	37 (40.7)	0.0152	(0.0024)	This
4340 (480°C)	173 (1195)	46 (50.6)	0.0200	(0.0032)	Study
4340 (550°C)	159 (1100)	54 (59.4)	0.0248	(0.0039)	
4340	204 (1410)	53 (58.2)	0.0214	(0.0034)	22
4340	216 (1490)	43.7 (48)	0.0172	(0.0027)	22
4340	206 (1420)	65 (71.5)	0.0262	(0.0041)	31
4340	220 (1520)	37.5 (41.2)	0.0146	(0.0023)	21
250 Maraging	246 (1700)	66 (72.5)	0.0242	(0.0038)	20
Average =			0.0205	(0.0033)	

Further Considerations

Considerably after these calculations had been made,[9] some experimental observations of the crack tip radius became available. Some light and scanning electron micrographs of the crack-tip radius, as measured under load, are shown in Fig. 11. These were then plotted as a function of K_I/σ_{ys} in Fig. 12. For three tempered conditions, the measured ρ seemed only to be a function of K_I/σ_{ys} as given by

$$\rho = \rho_0(K_I/\sigma_{ys}) \qquad [14]$$

where ρ_0 was a constant of 0.0015 $in^{1/2}$ (0.00022 $in^{1/2}$). This would affect stage II and III growth kinetics through a change in the plastic stress gradient, via Eq. [B-8]. If this had been used to assess stage II growth kinetics, one would have found

$$\left(\frac{da}{dt}\right)_{\mathrm{II}} \simeq \frac{3C_0D_A\overline{V}_{\mathrm{H}}\sigma_{ys}}{dRT(C_{cr} - C_0)} \ln\left[1 + \frac{d}{\rho_0(K_I/\sigma_{ys})}\right] \qquad [15]$$

One sees that this is nothing more than 2/3 times Eq. [9] times the log term. The value of $d/\rho_0(K/\sigma_{ys})$ is on the order of unity so that the actual magnitude is

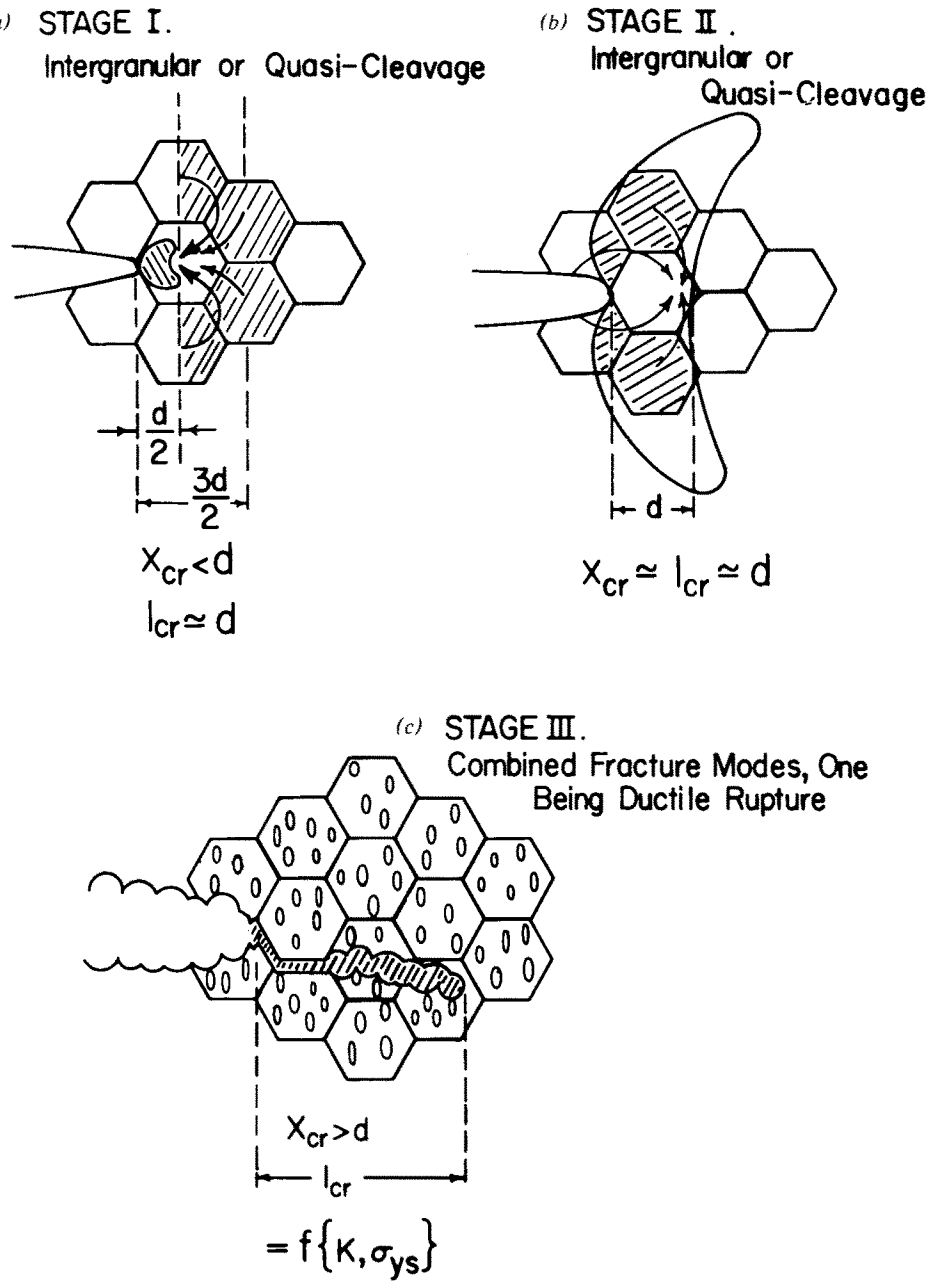

Fig. 8–Schematics of conditions loading to stage I, II, III crack growth. (Courtesy of ASM, Ref. 9).

Data Correlation

First consider the order of magnitude estimate of the crack growth rate using Eqs. [7] and [9] for stage I and stage II. With $RT/\bar{V}_H = 1.77\times 10^5$ psi (1220 MPa), $d \simeq 4\times 10^{-4}$ in. (10 μm), $\nu = 0.3$, $\sigma_{ys} = 2.08\times 10^5$ psi (1440 MPa) and $[C_0/C_{cr} - C_0)]D_A = 10^{-6}$ cm^2/s., stage I and II calculations compare reasonably well with the actual data in Fig. 9. That is, there are two regions, one stress intensity dependent and one stress intensity independent. The second curve shown in stage II will be discussed in a later section. One important point here is that the quantitative nature of the correlation is achieved primarily by the pick of the concentration-diffusivity term. Considering that the apparent diffusivity of hydrogen in iron and steel has been measured[17-19] to be from 2×10^{-8} to 2×10^{-5} cm^2/s, the estimate for $[C_0/(C_{cr} - C_0)]D_A$ is reasonable. It is possibly on the high side since one might expect a high strength steel to have a relatively high trap density[9] and hence tend toward a lower range of apparent diffusivities.

If the correlation technique is valid, then there must be a way of explaining the more than two order of magnitude shift in $(da/dt)_{II}$ for 4340 tempered at 550°C (823 K) *vs* 300°C (573 K). (See Figs. 3 and 10) This decrease cannot be explained in terms of an increased critical concentration required for lower strength conditions as was previously suggested for the threshold condition.[4] It could explain a factor of two or three difference but not several orders of magnitude. The decrease could be explained in terms of two possible tempering effects on D_A. That is, tempering could

(a) increase the number of effective traps such as precipitates which could give an order of magnitude effect.[9]

(b) increase the ease of deformation at the crack

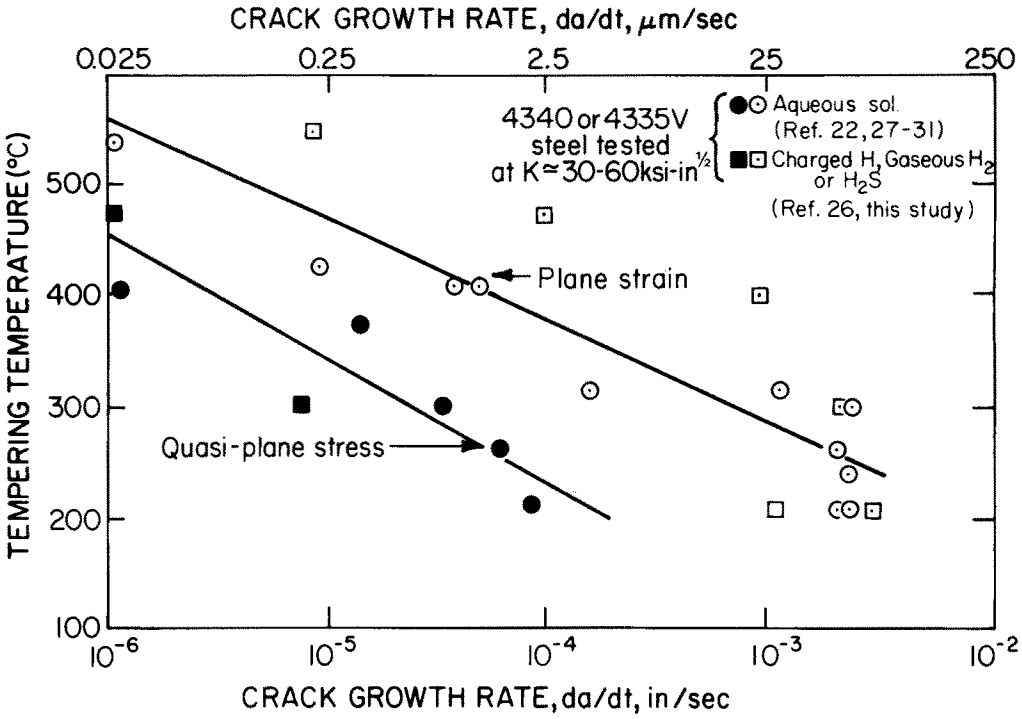

Fig. 10—Effect of tempering temperature on stage II crack growth rates. (Courtesy of ASM, Ref. 9).

nearly the same as predicted before. However, as K is increasing during stage II kinetics, Eq. [15] would no longer predict a K independent growth region but one where da/dt *decreases* with increasing K_I. This is illustrated by superimposing Eq. [15] on Fig. 9. Admittedly, the effect is small with the predicted decrease being on the order of a factor of two or less. Considering the wide swings in data often observed, *e.g.* Fig. 4, it is not surprising that such a reversal in da/dt might go undetected or ignored. Nevertheless, the data in Figs. 3, 4 and 5 did seem to indicate this effect. From other data plotted in a manner comparable to Fig. 5, da/dt at the start of stage II (with low K values denoted as K_L) was compared to da/dt near the end of stage II (with high K values denoted as K_H). From Eq. [15], it is seen that the ratio of da/dt at the start and end of stage II should be given by

$$\frac{(da/dt)_{K_L}}{(da/dt)_{K_H}} = \frac{\ln\left[1 + d\sigma_{ys}/\rho_0 K_L\right]}{\ln\left[1 + d\sigma_{ys}/\rho_0 K_H\right]} \qquad [16]$$

For all of the data, K_H was 38,000 psi-in$^{1/2}$ on the average. Using this value in conjunction with a σ_{ys} of 200,000 psi, a ρ_0 of 0.0014 in$^{-1/2}$ and a grain size of 10 μ, the dependence of da/dt could be described as a function of K_H/K_L. This was compared to the data of this investigation in Fig. 13. Data from Mostovoy, *et al*[20] are also shown. As there was a degree of uncertainty as to the grain size and crack-tip radius, a first order approximation to eliminate these parameters was made assuming for small x, $\ln(1+x) \simeq x$. Even though x is not that small in Eq. [16], it was useful since then

$$\frac{(da/dt)_{K_L}}{(da/dt)_{K_H}} \simeq \frac{K_H}{K_L} \qquad [17]$$

These two predictions are seen to compare reasonably well with the data in Fig. 13. They are also in qualitative agreement with Dunegan and Tetelman's[21] finding that at an applied stress intensity near 37,500 psi-in$^{1/2}$ (42 MPa-m$^{1/2}$), "island cracks" formed in front of the main crack and seemed to grow both ahead and back toward the man crack front. Associated with this was a slow down of the main crack. These observations would tend to verify the concept that the rate controlling step is hydrogen collecting near the elastic-plastic boundary as driven by the severity of the stress gradient.

It should be pointed out that others,[22-24] testing 4340 in aqueous solutions, found either constant or slightly increasing da/dt values in the stage II region. There is the additional problem of crack branching[25] which can occur near these stress intensity levels. Although not observed in the present investigation, this could cause cracks to slow down even though K_I is increasing. Obviously, this effect must be more carefully investigated to determine whether these second order variations in stage II are mostly experimental manifestations (*e.g.* heat to heat or test specimen variations) or ones of substance.

After the formulation of this paper, it was brought to our attention that recent elasto-plastic analyses have the location of the peak normal stress well within the plastic zone. For example, Rice *et al*[32,33] have shown that the peak stresses may occur at approximately $2\delta_t$ where δ_t is the crack-tip displacement. If this were completely plane strain, then $2\delta_t \simeq K^2/\sigma_{ys}E \simeq 3.8\,\mu$m or about a factor of four less than that estimated in Fig. 7. Although this would change the quantitative nature of some of the constants (*e.g.* by changing the limits of integration), it would not change the general approach indicated in Appendices A and B. It would tend to increase the pressure tensor gradient and hence the velocities in Eqs. [7], [9] and [11] by about a factor of four. This would simply necessitate decreasing $[C_0/(C_{cr} - C_0)]D_A$ by a factor of four to obtain the same fit in Fig. 9. In fact, this adjustment brings D_A into more realistic agreement with measured apparent diffusivities. This reinterpretation

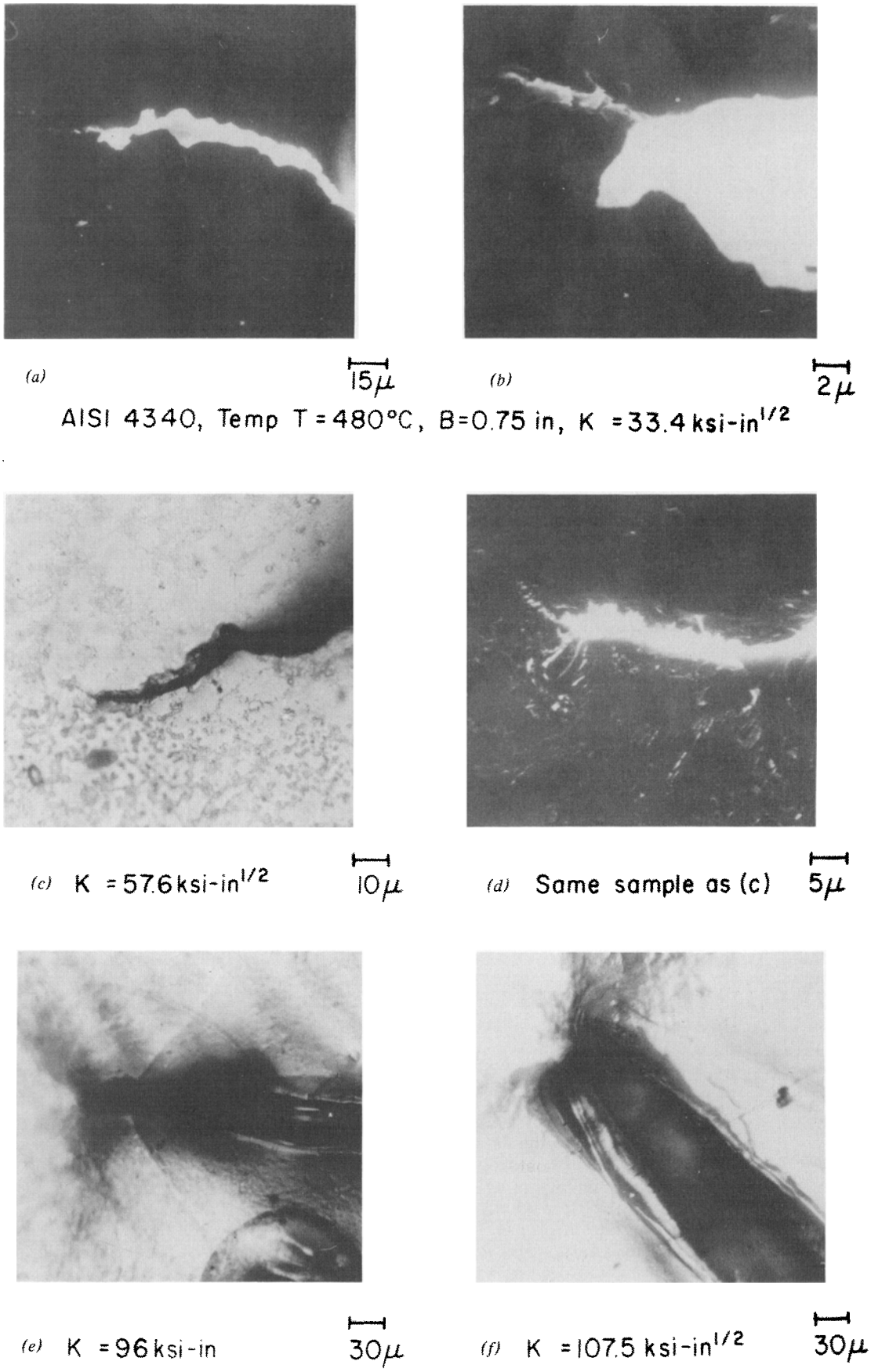

Fig. 11—Crack tip profiles as determined by scanning (*a*) (*b*) (*d*) and light (*c*) (*e*) (*d*) microscopy.

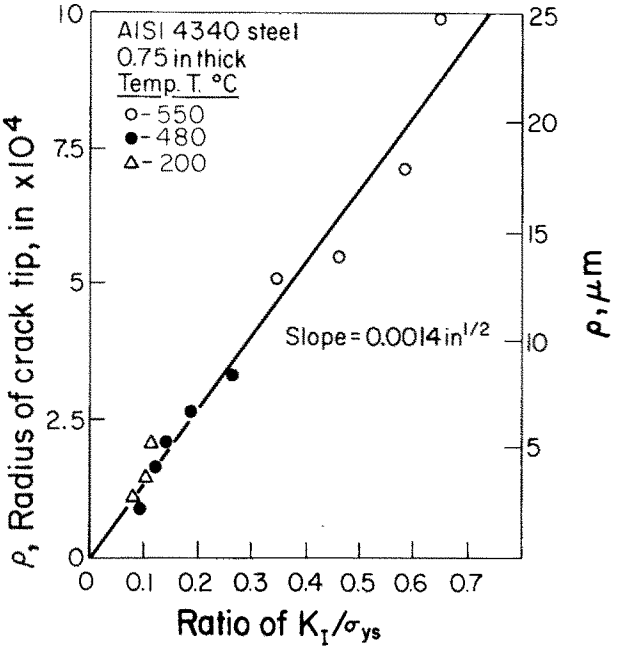

Fig. 12—Functional dependence of crack-tip radius on applied stress intensity.

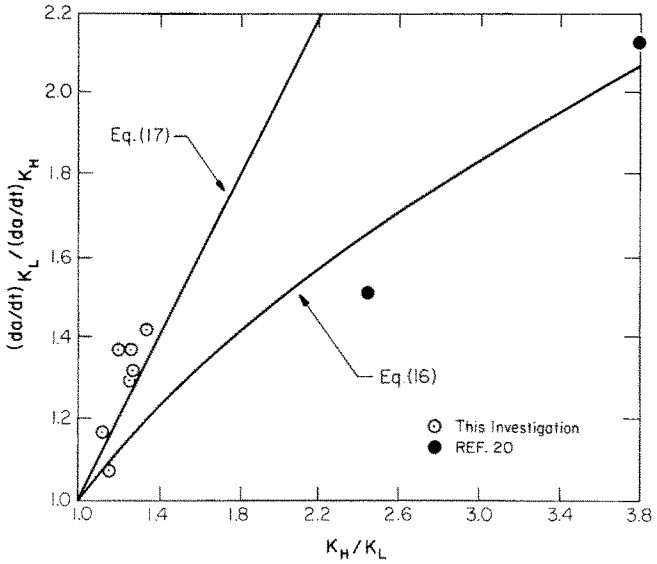

Fig. 13—Evaluation of crack-tip radius effect on stage II growth kinetics.

would not substantially affect the transitions associated with Eqs. [12] and [13] since it may be shown that both the elastic and plastic stress gradients would be increased by similar amounts. The one qualitative change would be the position at which hydrogen concentrates during stage II growth. This could be well within a grain but the size of the plastic zone would nevertheless be large enough to cause the plastic gradient to predominate. These results indicate that further analysis of the stress gradients and their corresponding effects on hydrogen flow and concentration are required.

Finally, some comment on how this interpretation compares to Oriani and Josephic's[34,35] concept of hydrogen-induced decohesion is in order. First, Oriani's model is essentially one of the hydrogen concentrating "elastically" in a region only a few atom layers beneath the crack tip. The lowering of the maximum cohesive force by large concentrations of hydrogen then triggers intergranular decohesion. This concept of elasticity very close to the crack tip is clearly not possible using either the present or Rice's elasto-plastic analyses.[32,33] Secondly, Oriani's equilibrium model predicts an atom by atom decohesion whereas the present approach envisions a grain by grain jump. Some additional verification of where the crack initiates and how it grows for cathodic, gaseous and aqueous environments is needed. Finally, we have made the first attempt at describing the hydrogen-induced crack velocity in a somewhat crude, but nevertheless organized framework of fracture mechanics.

CONCLUSIONS

1. Three distinct stages of crack growth, stages I, II and III, are observed during hydrogen-induced slow crack growth in 4340 steel.

2. The magnitudes of the crack velocity occurring during these three stages are progressively lowered by several orders of magnitude upon tempering to lower and lower strengths.

3. These three stages of crack growth can be correlated to a continuum fracture mechanics approach based primarily upon the pressure tensor gradient as the driving force for hydrogen diffusion in the vicinity of the crack tip.

4. Measurement of the transitions:

stage I to II—elastic stress gradient to plastic stress gradient (predominantly intergranular fracture)

stage II to III—intergranular fracture to ductile rupture fracture (predominantly plastic stress gradient)

are in good quantitative agreement with the continuum approach.

5. Measurements of crack-tip radii, ρ, indicate that ρ increases linearly with increasing stress intensity, K. When incorporated with the continuum model, it would predict that the driving force for hydrogen diffusion decreases with increasing K during stage II growth.

6. These later measurements, conducted after the original correlations had been made, imply a second order variation of crack growth rate, where $(da/dt)_{II}$ was found to *decrease* slightly with increasing stress intensity.

APPENDIX A

Short-time Diffusional Flow

First, consider a uniformly distributed hydrogen concentration, C_0. Then, consider hydrogen moving into a region in front of the crack to be driven by both elastic and plastic gradients. For short-time diffusion kinetics, Fick's first law of diffusion gives

$$v = \frac{D}{RT}\nabla u - D\frac{\nabla c}{c} \simeq \frac{D}{RT}\bar{V}_H\frac{dp}{dx} \qquad [A\text{-}1]$$

with the approximation on the right resulting if the concentration gradient is ignored. This leads to the very simplified picture schematically shown in Fig. A-1, if, within the crack plane, hydrogen flow is con-

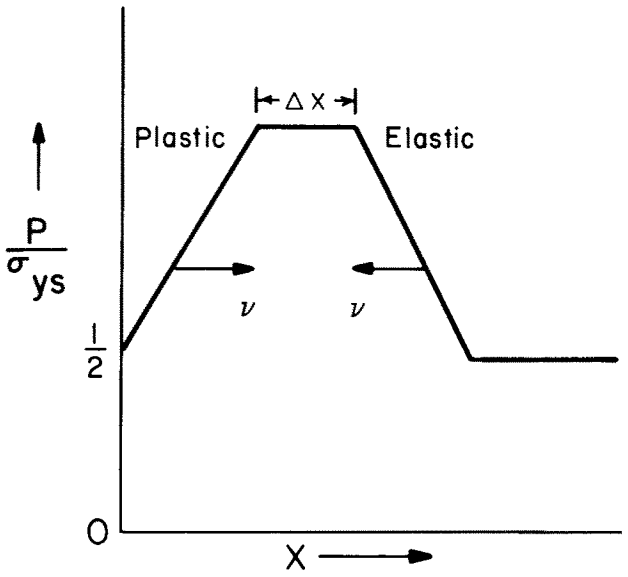

(a) STRESS FIELD

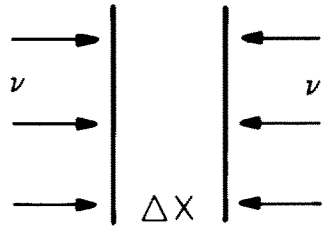

(b) HYDROGEN FLOW

Fig. A-1—Schematic of approximate stress fields and hydrogen diffusion at the tip of a crack.

sidered to be linear and parallel. In time, t, this would lead to a concentration build-up in the region Δx as given by

$$C_{\Delta x} = C_0 + \frac{2C_0 vt}{\Delta x} \qquad [A\text{-}2]$$

It may be shown that this crude first approximation is reasonable since a limited region outside Δx is contributing hydrogen to Δx. Consider this in somewhat more detail in terms of the way hydrogen drifts in an elastic stress field. The hydrogen paths are actually curved as was indicated in Fig. 8(a). These curved trajectories are orthogonal to the pressure tensor as indicated in Fig. A-2 for an elastic stress field. If the grains are contiguous to the crack tip, the path hydrogen would take would be relatively linear. However, at large distances the paths could be highly curved. Considering the elastic field paths in Fig. A-2, the concentration build-up to some critical concentration, C_{cr}, within a fracture region will depend upon the number of grains contributing hydrogen. Letting $C_{\Delta x} = C_{cr}$, $\Delta x = d$ and $t = \Delta t_s$, Eq. [A-2] becomes

$$C_{cr} = C_0 + \sum_i \frac{n_i C_0 v_i \Delta t_s}{d} \qquad [A\text{-}3]$$

where

v_i = average drift velocity in the i-th group of grains
n_i = number of grains in the i-th group.
Δt_s = time between crack jumps

Although it seems like one could have virtually any concentration build-up depending upon n_i, it must be noted that there are two limiting factors. The further hydrogen is from the crack tip, the further it has to move and the more slowly it moves since v_i decreases away from the crack tip according to Eqs. [A-1] and [B-3]. This effect can be clearly seen by examining three groups of grains (i = 1, 2, 3), each group being divided according to the average distance hydrogen would move along the curved paths indicated in Fig. A-2. These groups are depicted in Fig. A-3. What must be determined is whether there is sufficient time for the hydrogen in n_i grans to reach the crack tip. If we consider the slower crack velocities encountered, $da/dt \simeq 10^{-4}$ in./s, and the assumption that the crack grows one grain at a time, then $\Delta t_s \simeq d/(da/dt) \simeq 4$ s. One might point out that this is within about a factor of three of other Δt_s estimates made from stress-wave emission observations at similar crack velocities.[15] Taking this time and determining v_i from Eq.

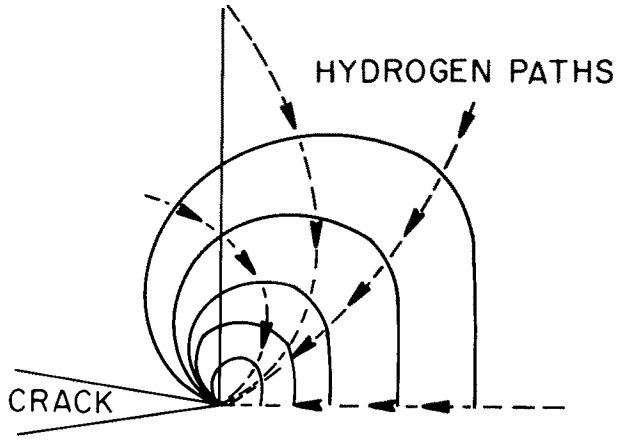

Fig. A-2—Hydrogen diffusion under an elastic Mode I stress field.

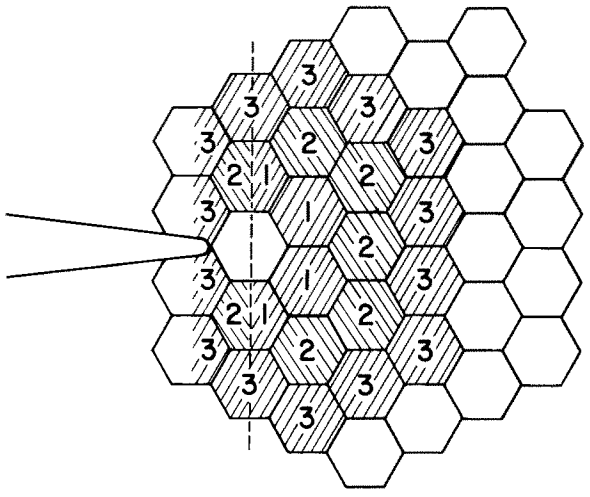

Fig. A-3—Possible groups of grains contributing hydrogen to the crack tip.

[A-1] using $D \simeq 3.18 \times 10^{-8}$ in^2/s (2×10^{-11} μm^2/s), $RT/V_H \simeq 1.77 \times 10^5$ psi (1220 MPa), and dp/dx from Eq. [B-3], the distance a hydrogen atom could move between crack jumps is:

for $i = 1$

$$x_1 \simeq \frac{3.18 \times 10^{-8} \text{ in.}^2/\text{s}}{1.77 \times 10^5 \text{ psi}} \times 2.72 \times 10^8 \text{ psi/in.} \times 4 \text{ s}$$
$$\simeq 1.96 \times 10^{-4} \text{ in.} \simeq 5 \ \mu\text{m}$$

for $i = 2$

$$x_2 \simeq \frac{3.18 \times 10^{-8} \text{ in.}^2/\text{s}}{1.77 \times 10^5 \text{ psi}} \times 1.27 \times 10^8 \text{ psi/in.} \times 4 \text{ s}$$
$$\simeq 0.91 \times 10^{-4} \text{ in.} \simeq 2.3 \ \mu\text{m}$$

for $i = 3$

$$x_3 \simeq \frac{3.18 \times 10^{-8} \text{ in.}^2/\text{s}}{1.77 \times 10^5 \text{ psi}} \times 0.76 \times 10^8 \text{ psi/in.} \times 4 \text{ s}$$
$$\simeq 0.545 \times 10^{-4} \text{ in.} \simeq 1.4 \ \mu\text{m}$$

Even if the combined diffusivity and secondary incubation time estimates were off by an order of magnitude, there would not be sufficient time for grains outside two grain diameters to contribute to the hydrogen concentration. Given the estimates above, it is conceivable that the second and third groups of grains could be contributing when $da/dt \simeq 10^{-5}$ in./s (0.25 μm/s) for the 550°C tempered condition. Nevertheless, for all other conditions, where $da/dt \geq 10^{-4}$ in./s (2.5 μm/s). the short-time diffusion kinetics are sufficiently rapid to put $n_i \simeq 3$ in Eq. [A-3] as used in Eq. [2] in the text. It would also suggest that v_i is the average drift velocity in the grains contiguous to the fracture as discussed in Appendix B.

APPENDIX B

Mean Value of dp/dx

The basic premises for utilizing the mean value theorem for the short time diffusion kinetics are

(i) The potential gradient of the stress field is the large factor controlling diffusion;

(ii) The contributing regions are small and the gradient does not vary a great deal over that region;

(iii) The contributing regions are either largely under the influence of an elastic or a plastic stress field.

Elastic Field Controlling. This corresponds to stage I growth, as depicted in Fig. 8(*a*), where it is proposed that the elastic region contributing hydrogen is large compared to the small plastic zone at the crack tip. Thus, the problem is treated purely in terms of the elastic stress field. The elastic stresses for a Mode I crack are given in terms of r, θ polar coordinates by[12]

$$\sigma_x = \frac{K_I}{(2\pi r)^{1/2}} \cos\frac{\theta}{2}\left[1 - \sin\frac{\theta}{2}\sin\frac{3\theta}{2}\right]$$

$$\sigma_y = \frac{K_I}{(2\pi r)^{1/2}} \cos\frac{\theta}{2}\left[1 + \sin\frac{\theta}{2}\sin\frac{3\theta}{2}\right]$$

$$\tau_{xy} = \frac{K_I}{(2\pi r)^{1/2}} \sin\frac{\theta}{2}\cos\frac{\theta}{2}\cos\frac{3\theta}{2}$$

$\sigma_z = 0$ for plane stress;

$\sigma_z = \nu(\sigma_x + \sigma_y)$ for plane strain

$$\tau_{xz} = \tau_{yz} = 0 \qquad \text{[B-1]}$$

The normal stress tensor at the tip of an opening mode crack under plane strain is thus

$$p = \frac{\sigma_{ii}}{3} = \frac{\sigma_1 + \sigma_2 + \sigma_3}{3} = \frac{\sigma_x + \sigma_y + \sigma_z}{3}$$
$$= \frac{(1+\nu)(\sigma_x + \sigma_y)}{3} = \frac{2(1+\nu)K_I}{3(2\pi r)^{1/2}} \cos\frac{\theta}{2} \qquad \text{[B-2]}$$

treating p as the hydrostatic *tension* or a negative hydrostatic pressure. Along the line of the crack at $r = x$, $\theta = 0$ deg, dp/dx would be given by

$$\frac{dp}{dx} = -\frac{K_I(1+\nu)}{3(2\pi)^{1/2}x^{3/2}} \qquad \text{[B-3]}$$

In general, it is obvious that for any particular r, θ, the pressure tensor gradient may be different. Furthermore, each hydrogen atom feeding into the crack tip would see an increasing dp/dx and experience an increasing velocity. Thus, there is an average velocity for each hydrogen atom. In addition, depending upon where the hydrogen atom is located, there would be a different distance over which it traveled; hence, each differently positioned hydrogen atom would have a different average velocity. At this stage of development, it is probably sufficient to treat a "typical" hydrogen atom as diffusing in from a distance $3d/2$ as suggested in Fig. 8(*a*). Thus, the mean velocity of the "typical" hydrogen atom would be

$$\overline{\frac{dp}{dx}} = \frac{1}{\frac{3d}{2} - \frac{d}{2}} \int_{\frac{d}{2}}^{\frac{3d}{2}} -\frac{K_I(1+\nu)}{3(2\pi)^{1/2}x^{3/2}}\,dx = -\frac{2K_I(1+\nu)}{9d^{3/2}} \qquad \text{[B-4]}$$

This is Eq. [6] as used in the text without the sign since it is the magnitude that is governing growth kinetics. The sign does indicate that the hydrogen atoms would be moving into the crack tip.

Plastic Field Controlling. Hill's slip-line field equation for plane strain, as given by Wang[13] are

$$\sigma_{x,y,z} = \sigma_{ys}\left[(0, 1, \tfrac{1}{2}) + \ln\left(1 + \frac{x}{\rho}\right)\right] \qquad \text{[B-5]}$$

Here, the digits in the first set of parentheses refer sequentially to the σ_{ii} stresses. Thus, the triaxial tension is

$$p = \frac{\sigma_{ii}}{3} = \frac{1}{3}[\sigma_x + \sigma_y + \sigma_z] = \sigma_{ys}\left[\ln\left(1 + \frac{x}{\rho}\right) + \frac{1}{2}\right] \qquad \text{[B-6]}$$

For this case, the stress gradient along the line of the crack would be

$$\frac{dp}{dx} = \frac{\sigma_{ys}}{\rho + x} \qquad \text{[B-7]}$$

Following the same argument as above for the elastic case, the mean velocity of the "typical" hydrogen atom in the plastic field depicted in Fig. 8(*b*) is given by

$$\overline{\frac{dp}{dx}} = \frac{1}{d-0}\int_0^d \left(\frac{\sigma_{ys}}{x+\rho}\right)dx = \frac{\sigma_{ys}}{d}\left[\ln\left(\frac{\rho+d}{\rho}\right)\right] \qquad \text{[B-8]}$$

At the start of stage II growth, K_I is on the order of $0.1\,\sigma_{ys}$ to $0.15\,\sigma_{ys}$ for the higher strength conditions shown in Fig. 3. Given this stress intensity variation, estimates[16] of the crack tip radius range from about 0.8×10^{-4} to 1.9×10^{-4} in. Since this is about $d/2$ to $d/5$ in terms of the grain size of this study, in the spirit of the estimate used, Eq. [B-8] becomes

$$\frac{\overline{dp}}{dx} \simeq \frac{3\sigma_{ys}}{2d} \qquad [B\text{-}9]$$

which is Eq. [8] in the text.

NOMENCLATURE

a	crack dimension
da/dt	crack growth rate
B	specimen thickness
C_0	initial concentration
C_{cr}	critical concentration
d	average grain diameter
D_A	apparent diffusivity
K_I	applied stress intensity
K_{TH}	threshold stress intensity
K_{ISCC}	stress corrosion threshold
K_{IC}	plane strain toughness
l_{cr}	crack jump size
P	pressure tensor
dp/dx	pressure tensor gradient
r_y	plastic zone radius
t_f	time to failure
Δt_s	time between jumps
v	solute drift velocity
$\bar{V}_H$	partial molal volume of hydrogen in Fe
W	specimen width
X	distance in front of tip
∇u	potential gradient
∇c	concentration gradient
ν	Poisson's ratio
ρ	crack-tip radius
$\sigma_{x,y,z}$	normal stress
σ_{ii}	normal stress tensor
σ_{ys}	uniaxial yield strength
I, II, III	crack growth stages

ACKNOWLEDGMENTS

This work was supported by the United States Atomic Energy Commission through Contract AT-11-1-2212.

REFERENCES

1. A. R. Troiano: *Trans. ASM*, 1960, vol. 52, p. 54.
2. R. A. Oriani: *Fundamental Aspects of Stress Corrosion Cracking*, p. 32, Nat. Assoc. of Corros. Engrs., Houston, 1969.
3. C. St. John and W. W. Gerberich: *Met. Trans.*, 1973, vol. 4, p. 589
4. W. W. Gerberich and Y. T. Chen: *Met. Trans.*, 1975, vol. 6A, p. 271.
5. B. C. Syrett: *Corrosion*, 1973, vol. 29, no. 1, p. 23.
6. H. P. Van Leeuwen: *ibid.*, no. 5, p. 197.
7. H. W. Liu: *J. Basic Eng., ASME*, 1970, vol. 92, p. 633.
8. R. P. Harrison, P. T. Heald, and J. A. Williams: *Scripta Met.*, 1971, vol. 5, p. 543.
9. W. W. Gerberich: *Hydrogen in Metals*, p. 115, ASM, Metals Park, 1974.
10. A. J. Stavros and H. W. Paxton: *Met. Trans.*, 1970, vol. 1, p. 3049.
11. W. G. Reuter and C. E. Hartbower: *Eng. Fract. Mech.*, 1971, vol. 3, p. 493.
12. P. C. Paris and G. C. Sih: *Amer. Soc. Test. Mater. Special Tech. Publ. 381*, 1965, p. 30.
13. A. J. Wang: *Quart. Appl. Mech.*, 1954, vol. 11, p. 427.
14. C. D. Beachem: *Met. Trans.*, 1972, vol. 3, p. 437.
15. W. W. Gerberich and C. E. Hartbower: *Fundamental Aspects of Stress Corrosion Cracking*, p. 420, Nat. Assoc. of Corros. Engrs., Houston, 1969.
16. A. S. Tetelman and A. J. McEvily, Jr.: *Fracture of Structural Materials*, John Wiley and Sons, New York, 1967.
17. F. R. Coe and J. Moreton: *Met. Sci. J.*, 1969, vol. 3, p. 209.
18. G. M. Evans and E. C. Rollason: *J. Iron and Steel Inst.*, 1969, December, p. 1491.
19. A. J. Kumnick and H. H. Johnson: *Met. Trans.*, 1974, vol. 5, p. 1199.
20. S. Mostovoy, H. R. Smith, R. G. Lingwall, and E. J. Ripling: *Eng. Fract. Mech.*, 1971, vol. 3, p. 291.
21. H. L. Dunegan and A. S. Tetelman: *Eng. Fract. Mech.*, 1971, vol. 2, p. 387.
22. C. S. Carter: *Corrosion*, 1969, vol. 25, no. 10, p. 423.
23. C. S. Carter: *Corrosion*, 1971, vol. 27, no. 11, p. 471.
24. V. J. Colangelo and M. S. Ferguson: *Corrosion*, 1969, vol. 25, no. 12, p. 509.
25. C. S. Carter: *Eng. Fract. Mech.*, 1971, vol. 3, p. 1.
26. G. E. Kerns and R. W. Staehle: *Scripta Met.*, 1972, vol. 6, p. 631.
27. W. D. Benjamin and E. A. Steigerwald: Air Force Materials Laboratory Report TR-68-80, 1968.
28. C. S. Kortovich and E. A. Steigerwald: *Eng. Fract. Mech.*, 1972, vol. 4, p. 637.
29. J. M. Krafft and H. L. Smith: NRL Memo Report 2598, Naval Research Laboratory, Washington, April 1973.
30. W. A. Van Der Sluys: *Eng. Fract. Mech.*, 1968, vol. 1, p. 447.
31. A. M. Sullivan: *Eng. Fract. Mech.*, 1972, vol. 4, p. 65.
32. J. R. Rice and M. A. Johnson: in *Inelastic Behavior of Solids*, M. F. Kanninen, *et al.*, ed, McGraw-Hill, New York, 1970, p. 641.
33. J. R. Rice and D. M. Tracy: in *Numerical and Computer Methods in Structural Mechanics*, S. J. Fenves, *et al.*, ed., Academic Press, New York, 1973, p. 585.
34. R. A. Oriani: *Bunsen-Gesellshaft Phys. Chem.*, 1972, vol. 76, p. 848.
35. R. A. Oriani: *Acta Met.*, 1974, vol. 22, p. 1065.